Probing magnetic anisotropy in epitaxial La_{0.67}Sr_{0.33}MnO₃ thin films and nanostructures via planar Hall effect

Le Zhang^a, Anil Rajapitamahuni^a, Yifei Hao^a, Xia Hong^{*a}

Dept. of Physics and Astronomy, University of Nebraska-Lincoln, 855 N. 16th St., Lincoln, NE

USA 68508-0299

ABSTRACT

The ability to control and manipulate magnetic anisotropy in the colossal magnetoresistive (CMR) oxide (La,Sr)MnO₃ (LSMO) is critical for its implementation in magnetic memory applications. In this work, we employ the planar Hall effect (PHE) as a powerful tool to probe the magnetic anisotropy in LSMO thin films and nanostructures, where the magnetization is too small to be detected by conventional magnetometry techniques. By analyzing the angular- and magnetic field-dependences of the PHE, we deduced an in-plane biaxial magnetocrystalline anisotropy (MCA) energy of ~1.2x10⁵ erg/cm² in LSMO thin films fully strained on (001) SrTiO₃ substrates. Creating nanoscale periodic depth modulation in LSMO establishes a uniaxial anisotropy with substantially enhanced MCA energy density, which is attributed to a high strain gradient sustained in the nanostructure. The energy competition between the biaxial and uniaxial MCA leads to multi-level resistance switching behavior in properly engineered LSMO nanostructures, which can be utilized to design the switching dynamics in magnetic memory devices. Our work points to the critical role of epitaxial strain in determining the MCA in CMR oxides, and provides an effective material strategy for engineering the magnetic properties of LSMO for novel spintronic applications with high thermal stability and high density data storage.

Keywords: Magnetic anisotropy, (La,Sr)MnO₃, strongly correlated oxides, epitaxial thin films, magnetic nanostructures, planar Hall effect, epitaxial strain, nonvolatile memory

1. INTRODUCTION

The colossal magnetoresistive (CMR) oxide (La,Sr)MnO₃ (LSMO) possesses large magnetoresistance and high spin polarization, making it a promising material candidate for developing magnetic field sensors and nonvolatile memory applications. When implemented in magnetic data storage devices such as magnetic tunnel junctions, a critical parameter that determines the thermal stability and switching dynamics of the device is the magnetic anisotropy. As the magnetocrystalline anisotropy (MCA) of bulk LSMO ($\sim 1.8 \times 10^4 \text{ erg/cm}^3$)⁶ is about one to two orders of magnitude lower than those for technology-relevant materials such as Fe ($4.8 \times 10^5 \text{ erg/cm}^3$) and Co ($5 \times 10^6 \text{ erg/cm}^3$), it is of high research interest to develop effective material strategies to engineering the MCA in LSMO for magnetic memory applications.

In this work, we have investigated the effect of epitaxial strain on the MCA in LSMO thin films, and developed a nanostructure approach to tailor the type and magnitude of the anisotropy energy in this material. Due to the small volume of the material system of interest, it is challenging to characterize the magnetization via conventional magnetometry technique such as SQUID. Instead, magnetotransport techniques such as the anisotropic magnetoresistance (AMR) and planar Hall effect (PHE) are known to depend sensitively on the magnetic energy landscape in magnetic conductors, 3,5,8-16 and can be utilized to quantitatively assesse the magnetic anisotropy in the system. Based on the PHE study, we deduced an in-plane biaxial anisotropy in LSMO thin films fully strained on SrTiO₃ (STO) substrates with the energy density of ~1.2x10⁵ erg/cm², consistent with the values reported in literature. We further demonstrated a uniaxial MCA with about 50-fold enhanced energy density in LSMO nanostructures with one-dimensional depth modulation, which is attributed to a strong strain gradient established in the nanostructures. By engineering the energy competition between the biaxial and uniaxial anisotropy, we also achieved multi-level resistance switching behavior. Our study reveals the critical role of epitaxial strain in determining the MCA in LSMO, which can be exploited to control and manipulate the magnetization switching dynamics in LSMO, paving the path for its implementation in novel spintronic devices such as magnetic tunnel junctions.

^{*}xia.hong@unl.edu; phone 1 402 472-2779; physics.unl.edu

2. MATERIAL PREPARATION AND CHARACTERIZATION

We deposited epitaxial La_{0.67}Sr_{0.33}MnO₃ thin films on (001) STO substrates using the off-axis radio frequency magnetron sputtering technique. The samples were deposited at 650 °C in Ar and O₂ process gas (120 mTorr total pressure, ratio of 2:1), and then cooled down in 1 atmosphere of O₂ to minimize the formation of oxygen vacancy. Bulk LSMO of this composition has a pseudo-cubic lattice constant of 3.87 Å,²⁰ subjected to a 0.9% tensile strain when deposited on STO. X-ray diffraction (XRD) scan shows (001) growth with *c*-axis lattice constant of 3.845 Å [Fig. 1(a)]. Atomic force microscopy (AFM) measurements reveal atomically smooth film surface with root-mean-square roughness of 1-2 Å. This is in line with the observation of Laue oscillations around the XRD Bragg peaks. By fitting to the oscillations, we have determined the film thickness. Figure 1(b) shows the temperature dependence of magnetization for a 5 nm LSMO film measured by SQUID. The magnetization corresponds to 3.06 μ_B /Mn at 100 K. At low temperature, magnetization increases to 3.2 μ_B /Mn. At the composition of x = 0.33, the optimal magnetization of LSMO is 3.67 μ_B /Mn. The lower value may be due to the existence of a magnetic dead layer.

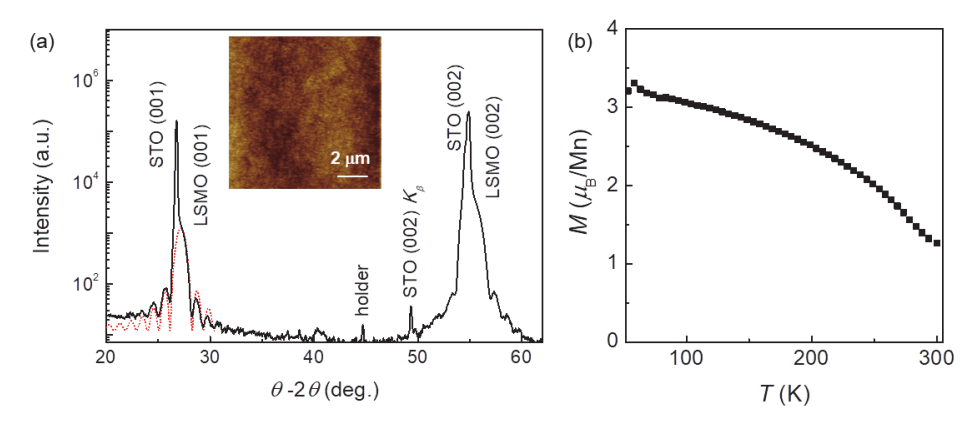


Figure 1. (a) X-ray θ -2 θ scan of a 10 nm LSMO sample grown on STO substrate. The red dashed line is a fit to the Laue oscillations. Inset: AFM topography image of a 6 nm LSMO film. (b) M(T) curve taken on a 5 nm LSMO with H = 5000 Oe // [110] direction of STO.

For the nanostructured samples, we fabricated the LSMO film into periodic depth modulation using electron beam lithography followed by fluorine-based reactive ion etching (RIE). As shown in Fig. 2(a), the top layered of LSMO was etched into periodic nano-stripes with a 1:1 width-separation ratio. The fabrication detail can be found in Ref. [16]. After etching the sample surface retains the smooth surface morphology with 2-3 Å roughness. For magnetotransport measurements, the samples were patterned into Hall bar devices, with the current along the [100] direction [Fig. 2(b)].

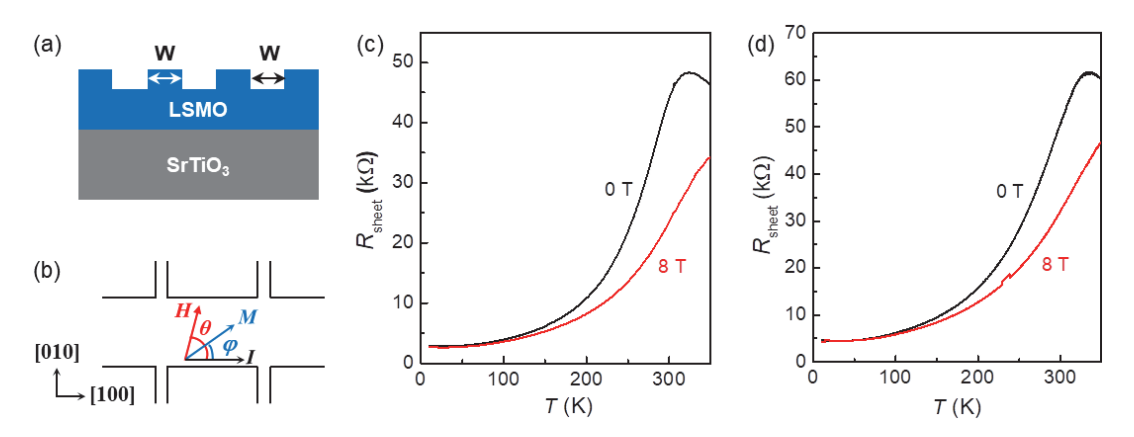


Figure 2. (a) Schematic cross-sectional view of the LSMO nanostructure. W = 100-250 nm. (d) Schematic view of the measurement geometry. (c) $R_{\text{sheet}}(T)$ for an unpatterned 7 nm LSMO film at 0 T and 8 T. (d) $R_{\text{sheet}}(T)$ for a 6 nm LSMO sample with the top layer patterned into 200nm width, 2 nm depth nano-stripes.

Figure 2(c) shows the sheet resistance $R_{\text{sheet}}(T)$ of an unpatterned LSMO film. The sample shows the characteristic temperature dependence of LSMO, transitioning from high temperature semiconducting behavior (dR/dT < 0) to low temperature metallic conduction (dR/dT > 0) as the sample going through the paramagnetic to ferromagnetic phase transition.²⁰ The resistance peak temperature T_p is around 325 K, close to the magnetic Curie temperature. At a magnetic field of 8 T, resistance decreases and T_p shifts to be above 350 K. We then measured $R_{\text{sheet}}(T)$ of a nanostructured LSMO [Fig. 2(d)], which exhibits very similar temperature dependence as the unpatterned film, proving that the RIE process does not cause noticeable damage to the sample quality.

3. PLANAR HALL EFFECT IN LSMO THIN FILMS

Next, we performed the PHE measurements to probe the magnetic energy landscape in LSMO thin films and nanostructures. For magnetic conductors, the resistivity measured as the current is parallel to the magnetization (ρ_{\parallel}) is often different from that obtained as the current is perpendicular to the magnetization (ρ_{\perp}). This effect can result in a transverse voltage in an in-plane magnetization, known as the planar Hall effect (PHE). The PHE resistivity exhibits a sinusoidal dependence on the angle φ between the in-plane magnetization and the current direction, as given by:⁸

$$\rho_{\text{PHE}} = (\rho_{\parallel} - \rho_{\perp}) \sin \varphi \cos \varphi. \tag{1}$$

Since the PHE signal in LSMO is orders of magnitude larger than that in ferromagnetic metals and not as sensitive to the CMR background as the anisotropic magnetoresistance, it is an ideal tool for high precision measurement of the magnetization orientation. 8,9

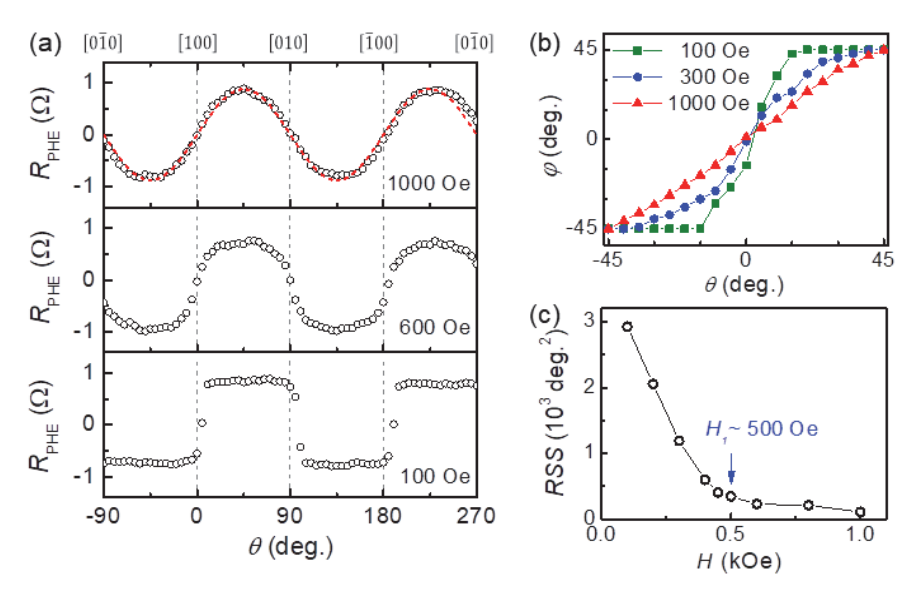


Figure 3. (a) R_{PHE} vs. θ taken on a 6 nm LSMO at H = 100 Oe, 600 Oe and 1000 Oe. The red dashed line is a fit to Eq. (1). (b) $\varphi(\theta)$ at different fields, and (c) the corresponding RSS plot taken on a 6 nm LSMO film. Data in (b)-(c) are from Ref. [16].

Figure 2(b) shows the experimental setup for the PHE measurement. In the experiment, we measure the Hall signal while varying the angle θ between the current and magnetic field. All PHE measurements were carried out at 100 K to achieve optimal signal. Figure 3(a) shows the PHE resistance R_{PHE} taken on a 6 nm LSMO thin film at different magnetic fields. We first set the sample in a single domain state by applying an in-plane magnetic field of 6 – 10 k Oe, and then measured R_{PHE} at constant fields while varying θ . At high magnetic fields (1 kOe), magnetization follows the direction of H, so that φ can be approximated by θ . The sample exhibit sinusoidal $R_{\text{PHE}}(\theta)$ that can be well described by Eq. (1). At a lower magnetic field of 600 Oe, magnetic anisotropy energy becomes comparable to the Zeeman energy, it is clear that $R_{\text{PHE}}(\theta)$ exhibits a distorted sinusoidal dependence, signaling that φ starts to deviate from θ (i.e. M does not fully follow H direction). As the field is further reduced to 100 Oe, R_{PHE} is clearly pinned to the two peak values, and

switches abruptly between the two plateaus states at $\theta = \pm n\pi/2$. This phenomenon, also known as the giant planar Hall effect, ^{8,9} is a direct manifestation of the strong magnetization pinning to one of the in-plane biaxial easy axes along <110>, consistent with what is expected for LSMO strained on (001) STO. ^{17,21,22} The sharp resistance switching is thus resulting from the magnetization switching between the two easy axes.

Assuming the sample is in a single domain state,²³ the evolving magnetization switching behavior can be understood within the coherent rotation model. The total free-energy density in the sample can be described by the Stoner-Wohlfarth model:⁷

$$F = K_u \sin^2\left(\varphi - \frac{\pi}{4}\right) + \frac{K_1}{4}\sin^2\left(\varphi - \frac{\pi}{4}\right) - MH\cos(\varphi - \theta). \tag{2}$$

Here, K_u and K_1 are the uniaxial and biaxial magnetic anisotropy constants, respectively. For LSMO thin films strained on STO, the first term is negligibly small.¹⁷ The last term describes the Zeeman energy within the magnetic field, which favors aligning M with H. The uniaxial and biaxial anisotropy fields H_u and H_1 are defined as $H_{u,1} = 2K_{u,1}/M$, which can be well approximated by the critical field for the system to evolve from the low field $\varphi \neq \theta$ regime to the high field $\varphi \approx \theta$ regime.^{7,8}

We identified the anisotropy field by quantitatively analyzing the relation between φ and θ . The angle φ can be extracted from Eq. (1) as $\varphi = \frac{1}{2}\sin^{-1}(R_{\text{PHE}}/R_{\text{PHE,max}})$. Figure 3(b) shows the $\varphi(\theta)$ data taken on a 6 nm LSMO film. Within the $\theta = [-45^{\circ}, 45^{\circ}]$ quadrant, φ exhibits strong pinning to $\pm 45^{\circ}$ at 100 Oe and a quasi-linear dependence at 1 kOe. We then evaluated the nonlinearity of $\varphi(\theta)$ by calculating the residual sum of squares (RSS) of its linear fit: $RSS = \sum_{i} [\varphi(\theta_i) - \theta_i]^2$. As shown in Fig. 3(c), RSS decreases rapidly with increasing H and approaches a saturated value at ~ 500 Oe, which is identified as H_1 . Using $H_1 = 2K_1/M$ and taking the magnetization value of 3.06 μ_B/Mn at 100 K [Fig. 1(b)], we deduced the biaxial anisotropy energy density to be $\sim 1.2 \times 10^5$ erg/cm³, comparable to previously reported values for LSMO on STO. $^{6,16-19}$

4. PLANAR HALL EFFECT IN LSMO NANOSTRUCTURES

We next fabricated depth modulated LSMO nanostructures with the nano-stripes along [010] direction, perpendicular to current [Fig. 2(a)], and carried out the PHE study. Figure 4(a) shows $R_{\rm PHE}(\theta)$ at 600 Oe taken on a 6 nm sample, where the top 2 nm was patterned into 200 nm width nano-stripes. Despite the similarity of the longitudinal resistance between the nanostructured and unpatterned LSMO [Fig. 2(c)-(d)], the PHE shows drastically different field dependence. At 600 Oe, which is already above the biaxial anisotropy field of the unpatterned sample, the patterned sample shows distinct $R_{\rm PHE}$ in the first and second quadrant, which are centered around [110] and [110], respectively. In the first quadrant, $R_{\rm PHE}$ shows sinusoidal θ -dependence similar to those on unpatterned LSMO. In sharp contrast, in the second quadrant, $R_{\rm PHE}$ remains to be pinned, signaling a much stronger anisotropy energy. The newly developed magnetic anisotropy is uniaxial along [110], as clearly manifested in the $\varphi(\theta)$ data [Fig. 4(b)]. By analyzing the linearity of $\varphi(\theta)$ at different magnetic fields [Fig. 4(c)], we identified a uniaxial anisotropy field H_u of ~5000 Oe, which is about 10-fold enhanced compared to the biaxial anisotropy field of unpatterned LSMO. Considering the nano-patterned region only constitute 20% of the sample volume, we concluded that the corresponding anisotropy energy density is about 50 times of that in LSMO thin films.

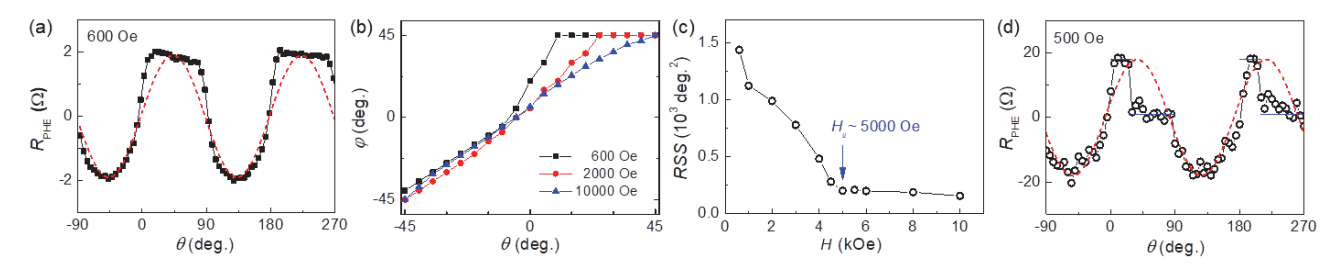


Figure 4. (a) R_{PHE} vs. θ at 100K, H = 600 Oe taken on a 6 nm LSMO with the top layer patterned into 200 nm width, 2 nm depth nano-stripes. (b) $\varphi(\theta)$ at different fields, and (c) the corresponding RSS plot taken on a 6 nm LSMO with the top

layer patterned into 200 nm width, 2 nm depth nano-stripes. Data in (b)-(c) are from Ref. [16]. (d) $R_{\rm PHE}$ vs. θ at 100K, H = 500 Oe taken on a 6 nm LSMO that is half patterned into 250 nm width, 1.2 nm depth nano-stripes. The red dashed lines are fits to Eq. (1). The blue solid lines serve as the guide to the eye.

Transmission electron microscopy studies of LSMO nanostructures shows that such modulation of the magnetic energy landscape can be well correlated with the a high strain gradient established within the nano-stripes, with c/a ratio progressively suppressed in the top-atomic layers by up to 10%. Modeling this unusual strain state using first principles density functional theory calculations has yielded a uniaxial MCA in orthorhombic LSMO strained on STO, successfully capturing both the orientation and magnitude of the emerging MCA.

The strain-modulated epitaxial nanostructure thus provides a versatile playground to control and manipulate the magnetic energy in LSMO, which can be utilized to tailor the functionalities of the material. As an example, in Fig. 4(d), we worked with a LSMO device where half of the current channel between the two Hall probes is patterned into periodic, 250 nm width, 1.2 nm depth nano-stripes, while the other half remains unpatterned. Following the sinusoidal θ -dependence of $R_{\rm PHE}$ in the first quadrant and the strong pinning of $R_{\rm PHE}$ at the beginning of the second quadrant, we observed an additional sharp switching in the PHE resistance to a new pinning state around $R_{\rm PHE} = 0~\Omega$. This behavior can be attributed to the strong energy competition between the biaxial MCA in the unpatterned area and the uniaxial MCA in the patterned area, which results in domain formation in the sample, yielding a net result of zero PHE.

5. CONCLUSIONS

In this work, we demonstrated that the planar Hall effect can be utilized as a powerful tool to quantitatively probe the magnetic anisotropy in epitaxial LSMO thin films and nanostructures, where the volume of the sample is too small to be characterized using conventional magnetometry techniques. We further showed that nanostructure engineering of the local strain state in LSMO can lead to substantially enhanced MCA and multi-state resistance switching. Our work thus provides important insight into the critical role of strain in determining the magnetic anisotropy in strongly correlated oxides, and points to a new route to the functional design of CMR oxides for novel spintronic applications.

We would like to thank Xuegang Chen and Balasubramanian Balamurugan for technical assistance. This work was supported by the National Science Foundation (NSF) under Grant No. DMR-1710461 (magnetotransport study and data analysis) and Grant No. DMR-1409622 (sample growth and characterization). The research was performed in part at the Nebraska Nanoscale Facility: National Nanotechnology Coordinated Infrastructure and the Nebraska Center for Materials and Nanoscience, which are supported by the NSF under Award ECCS: 1542182, and the Nebraska Research Initiative.

REFERENCES

- [1] Bibes, M., Villegas, J. & Barthelemy, A. "Ultrathin oxide films and interfaces for electronics and spintronics," *Adv. Phys.* **60**, 5-84 (2011).
- [2] Tsymbal, E. Y., Gruverman, A., Garcia, V., Bibes, M. & Barthelemy, A. "Ferroelectric and multiferroic tunnel junctions," *MRS Bulletin* 37, 138-143, doi:10.1557/mrs.2011.358 (2012).
- [3] Bason, Y. et al. "Planar Hall-effect magnetic random access memory," Journal of Applied Physics 99, 08r701, doi:10.1063/1.2162824 (2006).
- [4] Hoffman, J., Hong, X. & Ahn, C. H. "Device performance of ferroelectric/correlated oxide heterostructures for non-volatile memory applications," *Nanotechnology* **22**, 254014 (2011).
- [5] Hoffman, J. D., Wu, S. M., Kirby, B. J. & Bhattacharya, A. "Tunable Noncollinear Antiferromagnetic Resistive Memory through Oxide Superlattice Design," *Physical Review Applied* **9**, 044041, doi:10.1103/PhysRevApplied.9.044041 (2018).
- [6] Suzuki, Y. *et al.* "Magnetic anisotropy of doped manganite thin films and crystals," *Journal of Applied Physics* **83**, 7064-7066, doi:10.1063/1.367570 (1998).

- [7] Tannous, C. & Gieraltowski, J. "The Stoner-Wohlfarth model of ferromagnetism," *European journal of physics* **29**, 475 (2008).
- [8] Tang, H., Kawakami, R., Awschalom, D. & Roukes, M. "Giant planar Hall effect in epitaxial (Ga, Mn)As devices," *Physical review letters* **90**, 107201 (2003).
- [9] Bason, Y., Klein, L., Yau, J.-B., Hong, X. & Ahn, C. "Giant planar Hall effect in colossal magnetoresistive La_{0.84}Sr_{0.16}MnO₃ thin films. *Applied physics letters* **84**, 2593-2595 (2004).
- [10] Hong, X. et al. "Effect of electric field doping on the anisotropic magnetoresistance in doped manganites," *Physical Review B* 74, 174406, doi:10.1103/PhysRevB.74.174406 (2006).
- [11] Bason, Y. et al. "Planar Hall effect in epitaxial thin films of magnetite," Journal of Applied Physics 101, 09j507, doi:10.1063/1.2712053 (2007).
- [12] Yau, J. B. *et al.* "Anisotropic magnetoresistance in colossal magnetoresistive La_{1-x}Sr_xMnO₃ thin films," *Journal of Applied Physics* **102**, 103901, doi:10.1063/1.2811919 (2007).
- [13] Naftalis, N. *et al.* "Anisotropic magnetoresistance and planar Hall effect in epitaxial films of La_{0.7}Ca_{0.3}MnO₃," *Journal of Applied Physics* **106**, 023916, doi:10.1063/1.3176934 (2009).
- [14] Fina, I. et al. "Anisotropic magnetoresistance in an antiferromagnetic semiconductor," *Nature Communications* 5, 4671, doi:10.1038/ncomms5671 (2014).
- [15] Preziosi, D. et al. "Tailoring the interfacial magnetic anisotropy in multiferroic field-effect devices," *Physical Review B* **90**, 125155, doi:10.1103/PhysRevB.90.125155 (2014).
- [16] Rajapitamahuni, A. *et al.* "Giant enhancement of magnetic anisotropy in ultrathin manganite films via nanoscale 1D periodic depth modulation," *Physical review letters* **116**, 187201 (2016).
- [17] Steenbeck, K. & Hiergeist, R. "Magnetic anisotropy of ferromagnetic La_{0.7}(Sr, Ca)_{0.3}MnO₃ epitaxial films," *Applied Physics Letters* **75**, 1778-1780, doi:10.1063/1.124817 (1999).
- [18] Wang, Z. H., Cristiani, G. & Habermeier, H. U. "Uniaxial magnetic anisotropy and magnetic switching in La_{0.67}Sr_{0.33}MnO₃ thin films grown on vicinal SrTiO₃ (100)," *Applied Physics Letters* **82**, 3731-3733, doi:10.1063/1.1578711 (2003).
- [19] Tsui, F., Smoak, M. C., Nath, T. K. & Eom, C. B. "Strain-dependent magnetic phase diagram of epitaxial La_{0.67}Sr_{0.33}MnO₃ thin films," *Applied Physics Letters* **76**, 2421-2423, doi:10.1063/1.126363 (2000).
- [20] Urushibara, A. *et al.* "Insulator-metal transition and giant magnetoresistance in La_{1-x}Sr_xMnO₃," *Phys. Rev. B* **51**, 14103 (1995).
- [21] Lecoeur, P. et al. "Magnetic domain structures of La_{0.67}Sr_{0.33}MnO₃ thin films with different morphologies," *Journal of applied physics* **82**, 3934-3939 (1997).
- [22] Tsui, F., Smoak, M., Nath, T. & Eom, C. "Strain-dependent magnetic phase diagram of epitaxial La_{0.67}Sr_{0.33}MnO₃ thin films," *Applied Physics Letters* **76**, 2421-2423 (2000).
- [23] Wang, Z.-H., Cristiani, G. & Habermeier, H.-U. "Uniaxial magnetic anisotropy and magnetic switching in La_{0.67}Sr_{0.33}MnO₃ thin films grown on vicinal SrTiO₃ (100)," *Applied physics letters* **82**, 3731-3733 (2003).